A dual modal formulation for multiple flexural subsystems connected at a junction in energy-based models

Laurent Maxit, Oriol Guasch

A dual modal formulation for multiple flexural subsystems connected at a junction in energy-based models

Laurent Maxit[1] and Oriol Guasch[2]

1. INSA–Lyon, Laboratoire Vibrations-Acoustique (LVA), 25 bis, av. Jean Capelle, F-69621, Villeurbanne Cedex, France.

e-mail: laurent.maxit@insa-lyon.fr (corresponding author)

2. GTM - Grup de recerca en Tecnologies Mèdia, La Salle, Universitat Ramon Llull, C/ Quatre Camins 2, 08022 Barcelona, Catalonia, Spain.

e-mail: oriol.guasch@salle.url.edu

Abstract:

Statistical energy methods in vibroacoustics, like the statistical energy analysis (SEA) or the statistical modal energy distribution analysis (SmEdA), rely on specific modal coupling assumptions (MCAs) between subsystem modes. These methods assume that the behavior of subsystem mode amplitudes mimic that of oscillators, that the modes within a subsystem are uncoupled, and that the coupling between two different subsystems only takes place through the interaction of resonant modes. In the case of more than two subsystems being connected at a junction, however, it becomes difficult to establish a modal interaction scheme for them. In SEA, the problem is avoided by resorting to the travelling wave approach instead of the modal one. Nevertheless, there is a need for other energy-based methods, like SmEdA, to deal with such a situation. In this work it is proposed to extend the displacement-stress dual formulation, originally intended for two subsystems, to the case of multiple flexural waveguides connected at a junction. Numerical results are presented for a test case consisting of a floor coupled to two walls at right angle. The fulfillment of the MCAs by the dual modal formulation is examined in terms of the impedance mismatch between the floor and the walls.

Key words:

Statistical energy analysis, dual modal formulation, component modal synthesis, power flow, mid-frequency modelling, plate assembly

1 Introduction

Statistical energy-based approaches are widely used to describe the dynamics of complex built-up structures at *mid* and *high frequencies*. From all methods, the most popular one is statistical energy analysis (SEA) [1-5]. In SEA, the global system to be analyzed is subdivided into several subsystems (each one representing a group of resonant modes), and power balance equations are established between them. Despite their simplicity, the derivation of the SEA equations relies on several rigorous assumptions whose range of validity is not easy to establish. Many studies have addressed this subject in the past, see for example [6-11], or the more recent works in [12, 13].

The strict hypotheses demanded by SEA essentially confine it to the *high frequency* range. To address the so-called *mid-frequency* problem and extend energy-based methods to lower frequencies than those in the range of SEA, several proposals have been made. In the framework of modal approaches, the energy distribution analysis (EDA) [14], for instance, expresses the energy influence coefficients [15] of a built-up structure in terms of the modes of the whole structure. In the Asymptotical Scaled Modal Analysis (ASMA) method [16-19], the physical size of the solution domain is reduced based on a scaling law, while the damping loss factor is artificially increased. This leaves a scaled model that can represent the mean response of the original system, with the advantage of only needing a reduced number of modes.

Another modal approach is the statistical modal energy distribution analysis (SmEdA) method [20-22], which establishes power balance equations between individual connected subsystem modes, rather than between the subsystems themselves. This circumvents the SEA requirements of modal energy equipartition and enables applying SmEdA to cases of low modal overlap, locally excited subsystems, and to deal with complex heterogeneous subsystems. SEA is then recovered as a limiting case from SmEdA [20].

The coupling between two subsystems in SmEdA and SEA takes place according to a set of conditions that the resonant modes in the subsystems must fulfill. We may term such conditions as the modal coupling assumptions (MCAs), to be detailed below. The MCAs permit characterizing the coupling between subsystems (groups of resonant modes) in SEA, or between individual modes in SmEdA, through coupling loss factor coefficients.

The latter strongly facilitate solving SEA and SmEdA systems, and resolving problems of practical industrial interest, like the computation of energy transmission paths [23-26].

There is no evidence, however, indicating that the MCAs should generalize to multiple subsystems connected at a junction. It is precisely the purpose of this work to make some first steps towards this goal, by considering the case of several flexural waveguides sharing a common joint. As far as the authors know, this problem has not been tackled before.

In SEA, the latter seems to be a theoretical problem rather than a practical one. This is so because there is a way out to the situation: one can resort to the wave approach to SEA instead of the modal one. Travelling waves are considered and one can deduce the expressions for the coupling loss factors at a junction [27-30] from wave transmission coefficients [31-34]. Finite elements [35-36], spectral methods [37] and hybrid finite element (FEM)-SEA approaches [38] can also be employed to compute them. In SmEdA, however, the problem is not only of theoretical but also of practical importance. This is so because in SmEdA the subsystem modes are required to compute the coupling loss factors, and there is no alternative akin to the wave approach in SEA.

To find a modal coupling scheme for multiple subsystems connected at a junction, it is herein suggested to resort to the dual modal formulation (DMF) [39-42]. When applied to a pair of subsystems, the DMF complies with the MCAs. This formulation has been known since long ago to properly describe the dynamic behavior of a flexible structure coupled to a closed acoustic domain [39, 40]. The structure is described by the displacement field and the uncoupled-free modes (i.e. in-vacuo modes), whereas the cavity is characterized by the acoustic pressure field and the blocked modes (i.e. cavity modes assuming rigid walls).

By analogy between the acoustic waves in a fluid medium and the longitudinal waves in a rod, the DMF was extended in [41] to coupled rods, showing that the modal series converges even when the rods have equal properties. By the end of the nineties, the DMF was generalized to continuous mechanical systems [42]. If there is a mechanical impedance mismatch at a junction (which can be related to the weak coupling assumption), the modal series can be truncated to the resonant modes, as demanded by the MCAs [42]. The boundary conditions of the uncoupled-subsystems can then be clearly defined; the stiffest

subsystem should be free at the junction and described by its displacements, while the soft one should be blocked and represented by its stresses.

In this work, the DMF is extended to multiple subsystems sharing a junction. Still, the method requires one subsystem to be clearly stiffer than the others, the stiffest subsystem being characterized by its free modes and the remaining ones by blocked modes. Numerical tests will be presented for different impedance mismatches between subsystems, to determine under which conditions the resonant modes can represent the global behavior of the system, and therefore fulfill with the MCAs.

The paper is organized as follows. The MCAs are detailed in section 2, together with a summary of the DMF applied to a pair of subsystems. As a by-product of the paper, we also present a new derivation of the DMF equations in the Appendix, stemming from Hamilton's principle and its complementary form [43], rather than from Reissner's principle. Section 3 introduces a benchmark problem consisting of four panels sharing a junction, which will be used to facilitate discussion through the remaining of the paper. Some considerations on subsystem substructuring are also outlined, followed by the derivation of the DMF for the four panel test case. Numerical simulations and a discussion on the results are provided in section 4. The conclusions and future perspectives close the paper in section 5.

2 Basic theory for two coupled subsystems connected at a junction

2.1 Modal coupling assumptions

The modal coupling assumptions (MCAs) characterizing the interaction between modes, or groups of modes, belonging to two different subsystems, can be summarized as follows (see e.g., [1,5]):

- the interaction concerns the modes of the uncoupled subsystems,
- the dynamic behavior of a subsystem mode can be associated to the dynamic behavior of an oscillator (mass-spring-damper system),
- the coupling between the modes in different subsystems is conservative and takes place through mass, stiffness and/or gyroscopic elements,
- modes within a subsystem are uncoupled (orthogonality of modes),

- the resonant modes of each subsystem suffice to account for the energy interchanged with other subsystems.

Few works seem to exist analyzing the particular fulfilment of the MCAs in mechanical systems. Crandall and Lotz [20], for instance, established the modal equations for the specific case of two flexural beams coupled by a torsion spring. The subsystem modes were chosen as the modes of the uncoupled-free subsystems and displacements were used to describe the vibration of the two beams. However, the resulting modal coupling scheme was not in accordance with the MCAs; some terms arise in the formulation which express direct coupling between modes belonging to the same subsystem. Nonetheless, if the torsion stiffness of the spring is small in comparison with the beam flexural stiffness, it was shown that the inner mode coupling can be neglected leading to fulfillment of the MCAs. Scharton and Lyon had previously obtained similar results for two weakly coupled identical beams [44].

Despite of the MCAs being at the very core of SEA and SmEdA, as said in the Introduction it is unclear whether they could also apply to the connection of more than two subsystems. Before extending the DMF to multiple subsystems to check that issue, let us first give a summary of the method when applied to the easier situation of two coupled subsystems.

2.2 The dual modal formulation basic equations

Consider two continuous elastic subsystems 1 and 2, coupled at a junction Γ, subsystem 1 being excited by a mechanical force. The DMF [42] allows one to calculate the vibration response of the two coupled subsystems from the uncoupled subsystem modes and the reduced modal equations. In accordance with the formulation (see [42] and appendix A), the stiffer subsystem is described by its displacement field and its uncoupled-free modes (i.e. assuming null stresses at the connection), whereas the softer one should be characterized by a stress field (e.g., acoustic pressure) and by their uncoupled-blocked modes (i.e. contemplating null displacements at the connection).

Suppose that subsystem 1 is the stiffest one and that $\mathbf{u}_p$ represents the displacement vector of its p-th free mode when normalized to a unit modal mass. Besides,

$\boldsymbol{\sigma}_q$ stands for the stress tensor of the *q*-th blocked mode of subsystem 2, when normalized to unit modal stiffness (i.e. unit modal strain energy).

The displacement vector at a point *M* of subsystem 1, $\mathbf{u}(M,t)$, and the stress tensor at a point *N* of subsystem 2, $\boldsymbol{\sigma}(N,t)$, admit the modal expansions,

$$\mathbf{u}(M,t)=\sum_{p\in\hat{P}}\chi_p(t)\mathbf{u}_p(M) \quad \text{and} \quad \boldsymbol{\sigma}(N,t)=\sum_{q\in\hat{Q}}\xi_q(t)\boldsymbol{\sigma}_q(N), \tag{1}$$

where $\chi_p(t)$ and $\zeta_q(t)$ respectively represent the modal amplitudes. $\hat{P}$ and $\hat{Q}$ stand for the sets of modes of subsystems 1 and 2 retained in the modal expansion. The number of modes in each set are denoted by $P\equiv\text{card}\left[\hat{P}\right]$ and $Q\equiv\text{card}\left[\hat{Q}\right]$.

Following the DMF approach, the expressions in Eq. (1) are to be introduced in the weak formulation of the coupled problem. Taking advantage of the orthogonality of the uncoupled modes and making the change of variables $\dot{\zeta}_q=\xi_q, \forall q\in\hat{Q}$, the modal equations of motion can be written as (see appendix A for a derivation),

$$\begin{bmatrix}\mathbf{I} & \mathbf{0}\\ \mathbf{0} & \mathbf{I}\end{bmatrix}\begin{bmatrix}\ddot{\mathbf{q}}^1\\ \ddot{\mathbf{q}}^2\end{bmatrix}+\begin{bmatrix}\mathbf{0} & \mathbf{W}\\ -\mathbf{W}^T & \mathbf{0}\end{bmatrix}\begin{bmatrix}\dot{\mathbf{q}}^1\\ \dot{\mathbf{q}}^2\end{bmatrix}+\begin{bmatrix}\boldsymbol{\Lambda}^1 & \mathbf{0}\\ \mathbf{0} & \boldsymbol{\Lambda}^2\end{bmatrix}\begin{bmatrix}\mathbf{q}^1\\ \mathbf{q}^2\end{bmatrix}=\begin{bmatrix}\mathbf{f}^1\\ \mathbf{0}\end{bmatrix}, \tag{2}$$

with

$$\mathbf{q}^1=\left[\chi_p\right]_{P\times1},\ \mathbf{q}^2=\left[\zeta_q\right]_{Q\times1},\ \mathbf{f}^1=\left[F_p\right]_{P\times1},\ \mathbf{W}=\left[W_{pq}^{12}\right]_{P\times Q},$$
$$\boldsymbol{\Lambda}^1=\text{diag}\left[\omega_p^2\right]_{P\times P},\ \boldsymbol{\Lambda}^2=\text{diag}\left[\omega_q^2\right]_{Q\times Q}.$$

ω_p, ω_q denote the modal angular frequencies of modes *p* and *q*, and F_p the modal forces due to the external excitation. W_{pq}^{12} stands for the intermodal work between modes *p* and *q*, which is given by

$$W_{pq}^{12}=\int_\Gamma \mathbf{u}_p\boldsymbol{\sigma}_q\mathbf{n}\,\mathrm{d}\Gamma\ . \tag{3}$$

$\mathbf{n}$ in Eq. (3) represents the normal vector pointing outwards to the boundary of subsystem 2. Note that viscous damping could be also easily introduced in the modal equations (2).

The system of equations (2) corresponds well to the MCAs. In addition to the external force and the damping loss factor, these models require knowing the modal angular frequencies and the mode shapes (in term of displacements or stresses) at the coupling

junction. For time harmonic excitations, the modal amplitudes can be obtained solving the matrix system (2). The displacement at point *M*, or the stress at *N*, can then be computed from Eq. (1). Moreover, the total energy (kinetic energy + strain potential energy) of each subsystem can be calculated from the summation of their modal energies. The reader is referred to [42] for details on these developments, which will be not reproduced herein.

3 Extended theory for multiple subsystems connected at a junction

3.1 Description of the benchmark model and cases

For ease of exposition, the viability of the DMF approach when applied to multiple subsystems is analyzed for a specific structure composed of four flexural panels coupled at a junction, at right angle (see Fig. 1). Panels P1 and P2 in the figure represent the floor whereas panels P3 and P4 stand for vertical walls. The plates have clamped boundary conditions on the outer edges.

This example has been chosen because it is widely met in practical applications of SEA (e.g., in the naval and building industries). However, to keep the problem amenable for analytical description we have only considered the flexural motion of the panels. Therefore, the coupling among the plates only takes place through rotations and moments at the junction. The coupling between the out of plane motions (flexural) and the in-plane motions (longitudinal/shear motions) has been discarded in the analysis.

Two typical cases of building structures are contemplated. In the first one (test case #1), the floor is 20 cm in thickness and made of concrete, while the walls are 5 cm in thickness and made of brickwork. Therefore, there is a clear impedance mismatch at the junction, the concrete floor being much stiffer than the brickwork walls. In the second situation (test case #2), both, the floor and the walls will be made of concrete with a thickness of 20 cm. Consequently, all individual panels will have the same impedance.

A normal force excitation with unit power spectral density, $S_{FF}(f)=1\,\mathrm{N^2/Hz}$, is applied on panel P1, at the 1 kHz central frequency octave band. The point of excitation is located at coordinates (0m, 1.6m, 0.87m). The damping loss factor of the floor and walls has been fixed to 0.02 in both configurations.

The DMF calculations to be performed in subsequent sections need the subsystem modes as inputs, with appropriate boundary conditions. These modes have been computed

using the finite element method (FEM) and the SDTool code [45] in MATLAB. The computational mesh for test case #1 has been defined with a criterion of six elements per flexural wavelength at 2 kHz. The global FEM mesh is composed of 52126 nodes and 51604 quadrilateral shell elements, with 134 nodes belonging to the coupling junction. The same mesh has been considered for the second test case, which presents stiffer walls. Clamped boundary conditions have been imposed on the nodes of the outer edges. Moreover, the three translations remain blocked for the 134 nodes belonging to the coupling edge because, as said, only flexural motion has been taken into account. The meshes of the subsystems have been built from the global mesh. Appropriate boundary conditions at the nodes of the junction have been imposed in agreement with the requirements of the DMF method. The subsystem modes are then extracted using the Implicitly Restarted Lanczos Method (eigs command in SDTool, [45]). All subsequent DMF computations have been carried with MATLAB.

3.2 Sub-structuring and SEA weak coupling assumption

Once defined the test cases, the next step is that of partitioning the four-plate system into subsystems. This sub-structuring [46-50] should comply with the weak coupling assumption of SEA. Different definitions for the latter can be found in literature, which have always been a matter of discussion. The following ones could be useful in the present context.

In [46], Langley proposed that "*... the coupling will be said to be weak if the Green function for subsystem j is approximately equal to that of the uncoupled subsystem*.", while a few years later, Fahy and James [49] asserted that "*Under the conditions of weak coupling, the system modes are 'localized' in the sense that they closely resemble in natural frequency and shape the modes of the uncoupled subsystems (given the appropriate boundary conditions), and that their energies reside principally within the corresponding subsystems*.". Moreover, the same authors specified that "*Depending on the nature of the coupling, the boundary conditions for the uncoupled system do not always correspond to free displacement at the coupling*" [50].

The above considerations suggest that the localization of the global modes could give clear indications for partitioning a system into subsystems, as well as for defining the boundary conditions of the uncoupled subsystems. For example, in the EDA formalism

([14,16]), the ψ_{jk}^{r} parameter could be used as an indicator of localization of the global modes. This parameter corresponds to the integral on subsystem *r* of the product of mode shapes *i* and *j* multiplied by the mass density (see Eq. (3) in [16]). As global modes are considered in EDA, the ψ_{jj}^{r} parameter approaches to the generalized mass when the mode *j* is localized on subsystem *r*.

In the case of large models, localizing global modes for sub-structuring is not very practical because it implies computing all system modes. However, it provides a helpful guideline for our small four panel benchmark problem. For instance, in Fig. 2 we have plotted the spatial shapes of four global modes corresponding to the first test case of section 3.1, and compared them with the spatial shapes of the subsystem modes defined in accordance with the DMF. As observed from Figs. 2a and 2b, the global mode shapes at 80.4 Hz and 181 Hz are localized on panel P4, and closely resemble those of the uncoupled-blocked modes of panel P4 at 80.5 Hz and 181.1 Hz, shown in Figs. 2e and 2f. Similarly, the global mode shapes in Figs. 2c and 2d at 88.1 Hz and 308.9 Hz are mainly restricted to panels P1 and P2 (i.e., the floor) and match the floor uncoupled-free modes, as shown in Figs. 2g and 2h.

Altogether, this indicates that the DMF is well adapted to describe the vibration behavior of this system. The floor, which is the stiffest component, should constitute a single subsystem described in terms of displacements and by its uncoupled-free modes (null stress at the coupling junction). The vertical walls should be two additional independent subsystems characterized by their stresses and uncoupled-blocked modes (null displacement at the coupling junction). Therefore, in what follows subsystem 12 will designate the floor (panels P1 plus P2), whereas subsystems 3 and 4 will respectively correspond to the vertical walls P3 and P4.

3.3 Dual modal equations for the four panels

The DMF outlined in section 2.2 is next extended to the four-plate benchmark structure considering the subsystem partitioning presented above. Hereafter the following notation will apply:

- Γ_l designates the set of nodes belonging to the coupling junction,
- ω_p^{α} stands for the angular frequency of mode *p* of subsystem $\alpha \in \{12,3,4\}$,

- $\theta_{p,i}^{\alpha}$ and $M_{p,i}^{\alpha}$ respectively symbolize the angular rotation and reaction moment at node $i \in \Gamma_l$ of mode *p* of subsystem α.

As mentioned in section 3.1, the modes of each uncoupled subsystem have been calculated with FEM. Remember that to compact the equations, the mode shapes of subsystem 12 are taken normalized to unit modal kinetic energy and those of subsystems 3 and 4 normalized to unit modal strain energy. For subsystem 12, the three rotations of the 134 nodes belonging to the coupling junction have been left free whilst fixed to zero for subsystems 3 and 4.

Applying the DMF and the conditions of conservation of slope and bending moment at the junction, the modal equations for the 3 coupled subsystems can be deduced. These read, in matrix form,

$$\begin{bmatrix} \mathbf{I} & \mathbf{0} & \mathbf{0} \\ \mathbf{0} & \mathbf{I} & \mathbf{0} \\ \mathbf{0} & \mathbf{0} & \mathbf{I} \end{bmatrix} \begin{bmatrix} \ddot{\mathbf{q}}^{12} \\ \ddot{\mathbf{q}}^{3} \\ \ddot{\mathbf{q}}^{4} \end{bmatrix} + \begin{bmatrix} \mathbf{0} & \mathbf{W}^{12-3} & \mathbf{W}^{12-4} \\ -\mathbf{W}^{12-3\,\mathrm{T}} & \mathbf{0} & \mathbf{0} \\ -\mathbf{W}^{12-4\,\mathrm{T}} & \mathbf{0} & \mathbf{0} \end{bmatrix} \begin{bmatrix} \dot{\mathbf{q}}^{12} \\ \dot{\mathbf{q}}^{3} \\ \dot{\mathbf{q}}^{4} \end{bmatrix} + \begin{bmatrix} \mathbf{\Lambda}^{12} & \mathbf{0} & \mathbf{0} \\ \mathbf{0} & \mathbf{\Lambda}^{3} & \mathbf{0} \\ \mathbf{0} & \mathbf{0} & \mathbf{\Lambda}^{4} \end{bmatrix} \begin{bmatrix} \mathbf{q}^{12} \\ \mathbf{q}^{3} \\ \mathbf{q}^{4} \end{bmatrix} = \begin{bmatrix} \mathbf{F}^{1} \\ \mathbf{0} \\ \mathbf{0} \end{bmatrix} \qquad (4)$$

where

- $\mathbf{q}^{12}, \mathbf{q}^{3}, \mathbf{q}^{4}$ are the vectors of modal amplitudes of subsystems 12, 3, and 4 (q_p^{α} stand for their components, namely the *p*-th mode of the α-th subsystem),
- $\mathbf{\Lambda}^{12}, \mathbf{\Lambda}^{3}, \mathbf{\Lambda}^{4}$ are the eigenvalue diagonal matrices of subsystems 12, 3, and 4 (with only non-null components $\Lambda_{pp}^{\alpha\alpha} = \omega_p^2$), and,
- $\mathbf{W}^{12-3}$ and $\mathbf{W}^{12-4}$ are the matrices of intermodal works between subsystems 12 and 3, and between subsystems 12 and 4. Their components are designated by $W_{pq}^{\alpha\beta}$ (i.e., intermodal work between the *p*-th mode of subsystem α and the *q*-th mode of subsystem β) and can be computed from the FEM nodal variables as (see Eq. (80) in [42])

$$W_{pq}^{\alpha\beta} = \sum_{i \in \Gamma} \theta_{p,i}^{\alpha} M_{q,i}^{\beta} \,. \qquad (5)$$

Expanding one of the rows in Eq. (4) one gets a particular case of the canonical problem needed to comply with the MCAs [5],

$$\ddot{q}_p^{\alpha} + \omega_p^2 q_p^{\alpha} = F_p^{\alpha} + \sum_{\beta \neq \alpha} \sum_{q} W_{pq}^{\alpha\beta} \dot{q}_q^{\beta} \,, \tag{6}$$

which states that each mode *p* of a subsystem α behaves as a mass-spring oscillator (l.h.s of Eq. (6)) that is coupled to oscillators (modes *q*) in another subsystem $\beta \neq \alpha$ through gyroscopic elements (r.h.s of Eq. (6)). It remains yet to be checked whether the sole consideration of the subsystem resonant modes suffices to represent the global behavior of the system. In other words, is it possible to correctly estimate the subsystem energies if one only retains the resonant modes in the DMF Eq. (4)? To answer this question, DMF calculations will be performed in the following section with and without non-resonant modes and compared to a reference solution using the system global modes.

To compute the modal energy of the *p*-th mode of subsystem α, $E_p^{\alpha}(f)$, we have introduced some viscous damping in Eq. (4) and applied a unit harmonic excitation at frequency *f*. The vector of the modal energies of subsystem α, $\mathbf{E}^{\boldsymbol{\alpha}} = \left[\bar{E}_p^{\alpha} \right]$ can be computed from the modal amplitude vectors in Eq. (4) as,

$$\mathbf{E}^{\boldsymbol{\alpha}} = \frac{1}{2} \left(\omega^2 \mathbf{I} + \boldsymbol{\Lambda}^{\alpha} \right) \left| \mathbf{q}^{\alpha} \right|^2 . \tag{7}$$

The mean modal energy, $\bar{E}_p^{\alpha}$, in response to a white noise force of unit power spectral density in the octave band of central frequency f_c, is obtained by integrating (using a simple quadrature rule),

$$\bar{E}_p^{\alpha} = \int_{f_1}^{f_2} E_p^{\alpha}(f) S_{FF}(f) df = \int_{f_1}^{f_2} E_p^{\alpha}(f) df \,, \tag{8}$$

where f_1 and f_2 are the lower and upper bound frequencies of the considered octave band. On the other hand, the energy of subsystem α at frequency *f* can be computed adding the energies of the modes in the subsystem, $E^{\alpha}(f) = \sum_p E_p^{\alpha}(f)$. Finally, the subsystem energy

for a white noise force in the octave is computed as $\overline{E}^{\alpha} = \int_{f_1}^{f_2} E^{\alpha}(f)df$, which should equal $\sum_p \overline{E}_p^{\alpha}$.

4 Numerical simulations and discussion

4.1 Results

The total energies of subsystems 12 and 3 have been first calculated, according to the DMF, for the test case #1 of section 3.1, and plotted versus frequency in Fig. 3. This figure also contains the reference energies obtained from the global modes of the system, as described in section 2.2 of [51]. The calculations have been performed for the 1 kHz octave band considering 200 modes per subsystem. This frequency band has been initially chosen since it guarantees, at least, 10 resonant modes per band for each subsystem, as required by SEA [1,5].

A very good agreement can be observed between the different curves, even if only resonant subsystem modes are included in the DMF calculations. Some slight differences can also be appreciated at the bounds of the frequency band, which could be expected because of the stronger influence of the non-resonant modes at these frequencies. Note that the frequency matching between subsystem modes seems to have a similar effect than the one between global modes in EDA. Indeed, in the EDA formalism of [14,16], the frequency cross-modal terms Γ_{jk} are small unless modes *j* and *k* are resonant.

For better understanding the influence of neglecting the non-resonant modes, in Fig. 4 we have plotted the modal energies of each subsystem with and without considering them. The modal energies of subsystem 12 are not affected by the non-resonant modes (Fig. 4a), which is logical because subsystem 12 is directly excited with the external force. As opposed, non-resonant modes somewhat influence the less energetic modes of subsystems 3 and 4 (Figs. 4b and c), though the higher ones are well approximated only with the resonant modes. It can be therefore concluded that resonant coupling suffices for a correct prediction of the subsystem energies at the 1 kHz octave band.

One could wonder whether the above results would remain valid for other frequency bands and/or for different damping values. To that purpose further tests were

ran. Those are presented in Fig. 5. Three octave bands have been considered, namely 250 Hz, 500 Hz and again 1 kHz for comparison, as well as four damping loss factors that range from 0.005 to 0.05. The energies of the receiving subsystems 3 and 4 have been computed according to the DMF, with and without considering the non-resonant modes, and compared to the reference solution. Subsystem 3 respectively has 18, 40, and 101 resonant modes at the 250 Hz, 500 Hz and 1 kHz octave bands, while there are 15, 32 and 78 resonant modes for subsystem 4.

It can readily be checked from Fig. 5 that the DMF calculations well recover the reference energy of the receiving subsystems, even if one just considers the resonant modes. Notably, observe how the relatively low energy level of subsystem 4 at the 500 Hz octave band (as compared to the other two bands) is correctly represented by the DMF. The overall reduction of the two subsystem energies when increasing the damping is also well reproduced (see Figs. 5b, 5c and 5d). Meaningful differences can only be appreciated for subsystem 4 at 500 Hz, for the highest damping configuration (i.e. $\eta = 0.05$ in Fig. 5d). The subsystem energy is clearly underestimated in this case, particularly if non-resonant modes are neglected in the DMF computation. This can be attributed to the energy exchange between resonant and non-resonant modes having natural frequencies close to the upper and/or lower band limits of the octave. When the damping growths, the modal overlap factor increases and the interactions between subsystem modes are less sensitive to the frequency matching. The exchange of energy between resonant and non-resonant modes can then become significant. Except for that singular situation, however, it is apparent from Figs. 3, 4 and 5 that the results from the resonant DMF are quite satisfactory. Therefore, under the premises of test case #1, the DMF offers a modal coupling scheme in agreement with the MCAs.

Next, let us focus on test case #2 described in section 3.1. The same type of computations than for test #1 have been carried out. The results are summarized in Table 1, where the overall subsystem energies are presented. As observed, significant discrepancies with the global modes reference solution are found for subsystems 3 and 4, even if both, resonant and non-resonant modes are included in the computations. This means that the 200 - resonant or non-resonant - modes are not sufficient to ensure the convergence of the modal expansion and a larger number of them should be needed to

achieve a better result. In fact, this is not unexpected since the considered subsystem modes do not resemble those of the system global modes as in test case #1.

To better understand this point we may compare the subsystem modal parameters considered in the DMF with those of the global modes. These parameters are the modal frequencies f_p ($\omega_p = 2\pi f_p$) in Eq. (6)) and the modal angular rotations at the coupling junction, $\theta_{p,i}^{12}$, $i \in \Gamma$, in Eq. (5). Fig. 6, shows the values of the maximum angular rotation $\theta_p^{\max} = \max_{i \in \Gamma} \left| \theta_{p,i} \right|$ as a function of the modal frequencies f_p, up to 450 Hz. To facilitate visualization, only the free modes presenting a significant deformation of plate 1 have been included. One can observe how the values for subsystem 12 resemble those of the global modes for test case #1, which explains why convergence was achieved in that occasion. As opposed, the results for subsystem 12 clearly differ from the global ones for test case #2. The maximum angular rotations of subsystem 12 are systematically greater than those of the global system, whilst the modal frequencies become lower. Consequently, it is apparent that for the second test case the DMF seems not to be the appropriate approach to get a modal coupling scheme according to the MCAs.

4.2 Discussion

The basic reason for above behavior and failure of the DMF in case #2 is that the floor and the panels have the same thicknesses and material properties, and thus exhibit the same dynamic stiffness. Hence, a more pertinent partitioning scheme for #2 compliant with the DMF is needed.

One option could be that in Fig. 7a. It consists in choosing, for instance, panel P1 as a subsystem and then grouping all remaining panels into another subsystem. In such situation, there would be a significant mechanical impedance mismatch between the two subsystems and the DMF could be applied. Panel P1 (subsystem 1) could be well characterized by blocked modes, whereas the three others panels (subsystem 2) could be represented by free modes. However, this alternative sub-structuring would not be very feasible for complex built-up structures in practice, so it will be not pursued hereafter.

Test case	Energy \ Panel	1+2	3	4
#1	Reference	68.4 dB	44.7 dB	46.4 dB
#1	DMF	68.4 dB	44.2 dB	45.9 dB
#1	DMF (resonant modes only)	68.2 dB	44.0 dB	45.7 dB
#2	Reference	67.9 dB	56.6 dB	57.2 dB
#2	DMF	67.9 dB	37.7 dB	36.0 dB
#2	DMF (resonant modes only)	67.8 dB	34.8 dB	34.3 dB

Table 1: Comparison of subsystem energies for test cases #1 and #2. Role of resonant and non-resonant modes. Results correspond to the 1 kHz octave band (dB, ref. 10^{-12} J).

A more manageable sub-structuring alternative for case #2 could rely on the weak coupling definition by Fahy and James [49, 50], already cited in section 3.1. Given that all panels have the same dynamic stiffness, each one perceives the other three at the junction. One may therefore expect each panel to be blocked at the junction by the other three. The global modes could be more localized in that picture and resemble those of uncoupled panels with clamped boundary conditions at the junction. This would result in the sub-structuring scheme depicted in Fig. 7b, in which each panel is identified with a subsystem. Note that this scheme corresponds to the partitioning generally assumed in the traveling wave approach to SEA [27-30].

However, an important question remains, namely, which could be the modal formulation amenable with the partition scheme in Fig. 7b that also satisfies the MCAs? The DMF must be discarded because only one subsystem could be described by its uncoupled blocked modes, the other ones having to be characterized by uncoupled free modes. An appealing alternative would be to resort to the well-known Craig-Bampton (CB) method [52,53]. Given that the normal modes in the CB are defined with fixed-interfaces, this popular approach may be well adapted to our objective. Checking whether the CB, or some variation of it, is suitable to characterize multiple subsystems connected at a junction, with low impedance matching and according to the MCAs, will be the topic of companion paper [54].

5 Conclusions

In this paper we have studied the possibility of obtaining a modal coupling scheme for multiple flexural waveguides sharing a junction, in accordance with the required modal coupling assumptions (MCAs) of some energy-based methods, like SEA and SmEdA. In particular, the dual modal formulation (DMF) has been extended to deal with multiple connected subsystems. It has been shown that the latter can satisfy the MCAs, the modes of the different subsystems being coupled through gyroscopic elements. However, the DMF suffers from one drawback: it only works well if one of the subsystems is clearly stiffer than the others. Therefore, the approach fails when applied to subsystems with similar dynamic stiffness. This has motivated to address the problem of connected subsystems with low impedance mismatch in a companion paper [54].

On the other hand, we shall notice that only flexural waves have been considered in this work. Future developments may address the influence of longitudinal and shear waves on the modal coupling. Also, it would be interesting to derive coupling loss factors in SmEdA and SEA from the herein reported results.

Appendix A. Dual Modal Formulation from Hamilton's principle and its complementary form

A derivation of Eq. (2) in the main text steming from variational principles will be next presented. The reader is refered to [42] for a more complete description of all involved concepts and equations regarding the DMF. The exposition will be based on Hamilton's principle and its complementary form [43], while it was based on two forms of the Reissner principle in [42].

Let us consider two elastic continuous mechanic systems rigidly coupled at the surface Γ (see Fig. A.1). V_1 and V_2 represent the volumes occupied by subsystems 1 and 2, and the unit vectors n_1 and n_2 represent the outer normal to these volumes. Γ_α^F and $\Gamma_\alpha^C, (\alpha \in 1,2)$, respectively denote the boundary surfaces with free and blocked displacements. It is assumed that each subsystem is made of an elastic, homogeneous material.

In the following, subsystem 1 is described by its displacement field and subsystem 2 by its stress field. In Lagrangian coordinates $x_i, (\mathrm{i} = 1,2,3)$, u_i and ε_{ij} represent the

displacement and the strain tensor components in V_1, while σ_{ij} and p_i respectively denote those of the stress tensor and momentum in V_2. C_{ijkl} is the elasticity tensor associated to subsystem 1 and S_{ijkl} is the compliance tensor associated to subsystem 2. ρ_1 and ρ_2 respectively stand for the mass densities of subsystems 1 and 2. For the sub-structuring of the problem (see Fig. A.1), it becomes necessary to separate the two subsystems, and to prescribe displacements and stresses on their coupling surface Γ. The stress tensor components $\bar{\sigma}_{kl}$ are prescribed on Γ for subsystem 1, whereas the displacements $\bar{u}_l$ are imposed on Γ for subsystem 2.

The variational formulation of the elastodynamics of each subsystem can be introduced as follows. Consider the free vibration of the elastic conservative subsystems between time instants t_1 and t_2. For subsystem 1, described in terms of displacements, the Hamilton functional Π_H [43] reads,

$$\Pi_H(u_k) = \int_{t_1}^{t_2} \left\{ \int_{V_1} \left[T^* - U \right] dV + \int_{\Gamma} \bar{\sigma}_{ij} n_j^1 u_i d\Gamma \right\}, \tag{A.1}$$

where $U = \frac{1}{2}\varepsilon_{ij} C_{ijkl} \varepsilon_{kl}$ is the strain energy, with $\varepsilon_{ij} = \frac{1}{2}\left(u_{i,j} + u_{j,i}\right)$, and $T^* = \frac{1}{2}\rho_1 \dot{u}_i^{\,2}$ is the complementary kinetic energy. Here a comma denotes differentiation with respect to the index space coordinate. The dynamic problem related to subsystem 1 consists in finding the displacements u_i satisfying the displacement boundary conditions, which render the functional Π_H stationary.

The variational approach for subsystem 2, described in terms of stresses, involves the complementary form of Hamilton's functional, Π_T [43]. To express this functional in terms of σ_{ij}, one can consider the impulse quantities τ_{ij}, defined by $\dot{\tau}_{ij} = \sigma_{ij}$ (see [43]), so that

$$\Pi_T(\tau_{ij}) = \int_{t_1}^{t_2} \left\{ \int_{V_2} \left[U^* - T \right] dV + \int_{\Gamma} \bar{\dot{u}}_i \tau_{ij} n_j^2 d\Gamma \right\}. \tag{A.2}$$

$U^* = \frac{1}{2}\dot{\tau}_{ij} S_{ijkl} \dot{\tau}_{kl}$ in Eq. (A.2) is the complementary strain energy and $T = \frac{p_i^{\,2}}{2\rho_2}$ the kinetic energy, with $p_i = \tau_{ij,j}$ in the absence of volume forces. Solving the elastodynamics of

subsystem 2 consists in finding the impulses τ_{ij} that satisfy the force boundary conditions and render the functional Π_T stationary.

Next, let us consider the normal modes of the uncoupled-free subsystem 1 (i.e. with null stresses on Γ) and the normal modes of the uncoupled-blocked subsystem 2 (i.e. with null displacements on Γ). Denote by $u_{i,p}$ the displacement shapes (*i*=1,2,3) of mode *p* of the uncoupled-free subsystem 1, and by $\sigma_{ij,q}$ the stress shapes (*i,j*=1,2,3) of mode *q* of the uncoupled-blocked subsystem 2. The modal mass M_p, the modal stiffness K_p, and the modal angular frequency ω_p of mode *p* in subsystem 1, are given by

$$M_p = \int_{V_1} \rho_1 u_{i,p}{}^2 dV\,,\; K_p = \int_{V_1} \varepsilon_{ij,p} C_{ijkl} \varepsilon_{kl,p} dV\,,\; \omega_p = \sqrt{\frac{K_p}{M_p}}\,. \tag{A.3}$$

Analogously, the modal mass (or modal strain energy) M_q, the modal stiffness (or modal kinetic energy) K_q, and the modal angular frequency ω_q of mode *q* in subsystem 2, read

$$M_q = \int_{V_2} \sigma_{ij,q} S_{ijkl} \sigma_{kl,q} dV\,,\; K_q = \int_{V_2} \frac{\sigma_{ij,j,q}{}^2}{\rho_2} dV\,, \omega_p = \sqrt{\frac{K_q}{M_q}}\,. \tag{A.4}$$

The displacement field of subsystem 1 and the stress field of subsystem 2 can then be decomposed on their respective subsystem modal basis as,

$$u_i(M,t) = \sum_{p\in\hat{P}} \chi_p(t) u_{i,p}(M), \quad \sigma_{ij}(N,t) = \sum_{q\in\hat{Q}} \xi_q(t) \sigma_{ij,q}(N), \tag{A.5}$$

where χ_p and ζ_q represent the modal amplitudes, and $\hat{P}$, $\hat{Q}$ stand for the sets of modes of subsystems 1 and 2 retained in the modal expansion. Given that $\dot{\tau}_{ij} = \sigma_{ij}$, we can also decompose the impulse field as

$$\tau_{ij}(N,t) = \sum_{q\in\hat{Q}} \zeta_q(t) \sigma_{ij,q}(N) \text{ with } \dot{\zeta}_q = \xi_q, \forall q \in \hat{Q}. \tag{A.6}$$

Introducing the modal expansions Eqs. (A.5) and (A.6) in the functionals Eqs. (A.1) and (A.2), and making use of the orthogonality of modes (see [43]), provides the modal

amplitudes that render each functional stationary. This results in the Euler-Lagrange equations, which yield

$$\begin{cases} -M_p\ddot{\chi}_p - K_p\chi_p + \int_\Gamma \bar{\sigma}_{ij} n_j^1 u_{i,p} d\Gamma = 0, \forall p \in \hat{P}, \\ -M_q\ddot{\zeta}_q - K_q\zeta_q + \int_\Gamma \bar{\dot{u}}_i \sigma_{ij,q} n_j^2 d\Gamma S = 0, \forall q \in \hat{Q}. \end{cases} \tag{A.7}$$

To re-assemble the two subsystems, we impose displacement continuity and force equilibrium at the coupling surface Γ. This allows one to rewrite the prescribed displacements, $\bar{\dot{u}}_l$, and stresses, $\bar{\sigma}_{ij}$, on Γ as,

$$\bar{\dot{u}}_l(M,t) = \dot{u}_i(M,t),\ M \in \Gamma, \tag{A.8}$$

$$\bar{\sigma}_{ij}(M,t) n_j^1 = -\sigma_{ij}(M,t) n_j^2, M \in \Gamma. \tag{A.9}$$

From the modal expansions in Eq. (A.5) it follows

$$\bar{\dot{u}}_l(M,t) = \sum_{p\in\hat{P}} \dot{\chi}_p(t) u_{i,p}(M),\ M \in \Gamma, \tag{A.10}$$

$$\bar{\sigma}_{ij}(M,t) n_i^1 = -\sum_{q\in\hat{Q}} \xi_q(t) \sigma_{ij,q}(M) n_j^2 = -\sum_{q\in\hat{Q}} \dot{\zeta}_q(t) \sigma_{ij,q}(M) n_j^2,\ M \in \Gamma. \tag{A.11}$$

Introducing Eqs. (A.10) and (A.11) in Eq. (A.7), finally results in

$$\begin{cases} M_p\ddot{\chi}_p + K_p\chi_p + \sum_{q\in\hat{Q}} W_{pq}^{12} \dot{\zeta}_q = 0, \forall p \in \hat{P}, \\ M_q\ddot{\zeta}_q + K_q\zeta_q - \sum_{p\in\hat{P}} W_{pq}^{12} \dot{\chi}_p = 0, \forall q \in \hat{Q}, \end{cases} \tag{A.12}$$

with $W_{pq}^{12} = \int_\Gamma u_{i,p} \sigma_{ij,q} n_j^2 d\Gamma$ standing for the intermodal work between mode *p* in subsystem 1 and mode *q* in subsystem 2. Eq. (2) in the main text is nothing but Eq. (A.12) written in matrix form and normalized to unit modal mass.

REFERENCES

[1] R.H. Lyon, R.G. Dejong, *Theory and application of statistical energy analysis,* Second ed. – Boston: Butterworth-Heinemann, 1995. 277p.

[2] E.E. Ungar, Fundamentals of statistical energy analysis of vibrating systems, US Air Force AFFDL-TR 66–52, April, 1966.
[3] J. Woodhouse, An approach to the theoretical background of statistical energy analysis applied to structural vibration, The Journal of the Acoustical Society of America, 69 (1981) 1695-1709.
[4] C.B. Burroughs, R.W. Fischer, F.R. Kern, An introduction to statistical energy analysis, The Journal of the Acoustical Society of America 101 (1997) 1779–1789.
[5] A. Le Bot, Foundation of statistical energy analysis in vibroacoustics, First ed. Oxford University Press, Oxford, UK, 2015.
[6] A. Sestieri, A. Carcaterra, Vibroacoustics: The challenges of a mission impossible? Mechanical Systems and Signal Processing 34 (2013) 1-18.
[7] A. Culla, A. Sestieri, Is it possible to treat confidentially SEA the wolf in sheep's clothing? Mechanical Systems and Signal Processing 20 (2006) 1372-1399.
[8] A.J. Kean, W.G. Price, Statistical energy analysis of strongly coupled systems, Journal of Sound and Vibration 117 (1987) 363–386.
[9] B.R. Mace, On the statistical energy analysis hypothesis of coupling power proportionality and some implications of its failure, Journal of Sound and Vibration 178 (1994) 95–112.
[10] S. Finnveden, Ensemble averaged vibration energy flows in a three-element structure, Journal of Sound and Vibration 187 (1995) 495–529.
[11] F.F. Yap, J. Woodhouse, Investigation of damping effects on statistical energy analysis of coupled structures, Journal of Sound and Vibration 197 (1996) 351–371.
[12] A Le Bot and V. Cotoni. Validity diagrams of statistical energy analysis. Journal of sound and vibration 329 (2) (2010) 221-235.
[13] T. Lafont, N. Totaro, and A. Le Bot. Review of statistical energy analysis hypotheses in vibroacoustics. Proceedings of the Royal Society A. 470 (2014) 20130515.
[14] B. Mace, Statistical energy analysis, energy distribution models and system modes, Journal of Sound and Vibration, 264 (2003) 391-409.
[15] J.L. Guyader, C. Boisson, C. Lesueur, Energy transmission in finite coupled plates, Part I: theory, Journal of Sound and Vibration 81 (1982) 81–92.

[16] S. De Rosa, F. Franco, A scaling procedure for the response of an isolated system with high modal overlap factor, Mechanical Systems and Signal Processing, 22 (2008) 1549-1565.
[17] S. De Rosa, F. Franco, On the use of the asymptotic scaled modal analysis for time-harmonic structural analysis and for the prediction of coupling loss factors for similar systems, Mechanical Systems and Signal Processing, 24 (2010) 455-480.
[18] S. De Rosa, F. Franco, T. Polito, Structural similitudes for the dynamic response of plats and assemblies of plates, Mechanical Systems and Signal Processing, 25 (2011) 969-980.
[19] S. De Rosa, F. Franco, X. Li, T. Polito, A similitude for structural acoustic enclosures, Mechanical Systems and Signal Processing, 30 (2012) 330-342.
[20] L. Maxit, J.L. Guyader, Extension of SEA model to subsystem with non-uniform modal energy distribution, Journal of Sound and Vibration, 265, 337-358, 2003.
[21] N. Totaro, J.L. Guyader, Extension of the statistical modal energy distribution analysis for estimating energy density in coupled subsystems, Journal of Sound and Vibration, 331 (2012) 264-289.
[22] L. Maxit, K. Ege, N. Totaro, J.L. Guyader, Non-resonant transmission modelling with statistical modal energy distribution analysis, Journal of Sound and Vibration 333 (2014) 499–519.
[23] O. Guasch and À. Aragonès, Finding the dominant energy transmission paths in statistical energy analysis. Journal of Sound and Vibration, 330 (2011) 2325-2338.
[24] O. Guasch, A. Aragonès, M. Janer, A graph cut strategy for transmission path problems in statistical energy analysis. Mechanical Systems and Signal Processing, 30 (2012) 343-355.
[25] A. Aragonès, O. Guasch, Ranking paths in statistical energy analysis models with non-deterministic loss factors, Mechanical Systems and Signal Processing 52-53 (2015) 741-753.
[26] À. Aragonès, L. Maxit and O. Guasch, A graph theory approach to identify resonant and non-resonant transmission paths in statistical modal energy distribution analysis. Journal of Sound and Vibration 350 (2015) 91-110.

[27] S.H. Crandall, R. Lotz, On the coupling loss factor in statistical energy analysis. *The Journal of the Acoustical Society of America*, 49 (1) (1971) 352-356.

[28] M.J. Crocker, A.J. Price, Sound transmission using Statistical Energy Analysis, *Journal of Sound and Vibration*, 9 (1969), 469–486.

[29] R.S. Langley, P.J. Shorter, The wave transmission coefficients and coupling loss factors of point connected structures, *Journal of the Acoustical Society of America* 113 (2003) 1947-1964.

[30] C. Díaz-Cereceda, J. Poblet-Puig, A. Rodríguez-Ferran, Numerical estimation of coupling loss factors in building acoustics, *Journal of Sound and Vibration*, 332 (2013) 5433 – 5450.

[31] D.B. Pedersen, Estimation of vibration attenuation through junctions of building structures, *Applied Acoustics*, 46 (1995), 285–305.

[32] P.G. Craven, B.M. Gibbs, Sound transmission and mode coupling at junctions of thin plates, part 1: representation of the problem, *Journal of Sound and Vibration*, 77 (1981), 417-427.

[33] B.M. Gibbs, Mode coupling and energy partition of sound in a system of plate junctions, *Journal of Sound and Vibration*, 104 (1986) 127-136.

[34] R.S. Langley, Elastic wave transmission coefficients and coupling loss factors for structural junctions between curved panels, *Journal of Sound and Vibration,* 169 (1994), 297-317.

[35] J.A. Steel, R.J.M. Craik, Statistical energy analysis of structure-borne sound transmission by finite element methods, *Journal of Sound and Vibration*, 178 (1994), 553–561.

[36] C. Simmons, Structure-borne sound transmission through plate junctions and estimated of SEA coupling loss factors using the finite element method, *Journal of Sound and Vibration*, 144 (1991) 215-227.

[37] J. Poblet-Puig, C. Guigou-Carter, Using spectral finite elements for parametric analysis of the vibration reduction index of heavy junctions oriented to flanking transmissions and EN-12354 prediction method, *Applied Acoustics*, 99 (2015) 8–23.

[38] V. Cotoni, P. Shorter, R. Langley, Numerical and experimental validation of the hybrid finite element-statistical energy analysis method, *Journal of the Acoustical Society of America*, 122 (2007) 259-270.
[39] F. Fahy, Vibration of containing structures by sound in the contained fluid. Journal of Sound and Vibration, 10 (1969) 490-512.
[40] F. Fahy, Response of a cylinder to random sound in the contained fluid, Journal of Sound and Vibration, 13 (1970) 171-194.
[41] D. Karnopp, Coupled vibratory-system analysis, using the dual formulation. *The* Journal of the Acoustical Society of America, 40 (1966) 380-384.
[42] L. Maxit, J.-L. Guyader, Estimation of SEA coupling loss factors using a dual formulation and FEM modal information. Part I: Theory, Journal of Sound and Vibration, 5 (2001) 907-930.
[43] B. Tabarrok, Complementary variational principles in elastodynamics, Computers & structures, 19 (1984) 239-246.
[44] T.D. Scharton, R.H. Lyon, Power flow and energy sharing in random vibration. Journal of the Acoustical Society of America, 43 (1968) 1332-1343.
[45] E. Balmes, Structural Dynamics Toolbox & FEM link, User's guide, SDTools, Paris, France, 2011.
[46] R.S. Langley - A general derivation of the statistical energy analysis equations for coupled dynamic systems. Journal of Sound and Vibration, 135 (1989) 499-508.
[47] C. Diaz-Cereceda, J. Poblet-Puig, A. Rodriguez-Ferran, Automatic subsystem identification in statistical energy analysis, Mechanical Systems and Signal Processing 54-55 (2015) 182-194.
[48] F.X. Magrans, J. Poblet-Puig, A. Rodriguez-Ferran, A subsystem identification method based on the path concept with coupling strength estimation, Mechanical Systems and Signal Processing 100 (2018) 588-604.
[49] F. Fahy, P. James, An indicator of coupling strength between SEA subsystems. In: *IUTAM symposium on Statistical Energy Analysis*. - Southampton, UK: ISVR, University of Southampton, July 1997, p. 233-244.

[50] F. Fahy, P. James, A study of the kinetic energy impulse response as an indicator of the strength of coupling between SEA subsystems, Journal of Sound and Vibration, 190 (1996) 363-386.
[51] B.R. Mace, P. Shorter, Energy flow models from finite element analysis, Journal of Sound and Vibration, 233 (2000) 369-389.
[52] R. Craig, C.J. Chang, Substructure coupling for dynamic analysis and testing, NASA CR-2791, Washington, DC, 1977.
[53] C. Pierre, Mid-frequency dynamics of complex structural system: assessing the state of the art and defining future research directions, Air Force Office of Scientific Research, Arlington, USA, Report 20030115 102, 2002.
[54] L. Maxit, O. Guasch, Energy-based reformulated Craig-Bampton method for multiple flexural subsystems connected at a junction with low impedance mismatch, Mechanical Systems and Signal Processing, Submitted (2018).

FIGURE CAPTIONS

Figure 1. Geometry of the benchmark structure.

Figure 2. Comparison of the spatial shapes of the system global modes (left column) and the subsystem modes computed with the DMF (right column) for the first test case. (a-d) examples of global modes; (e-f) blocked modes of P4: (g-h) free modes of P1+P2.

Figure 3. Subsystem energy response depending on frequency for subsystem 12 (black) and subsystem 3 (grey), for test case #1. Continuous line: reference energy from global modes; Dashed line: DMF computation considering resonant and non-resonant modes; Dotted line: DMF computation with only resonant modes.

Figure 4. Modal energy distribution for test case #1. Cross: DMF taking into account resonant and non-resonant modes; Circle: DMF only considering resonant modes; (a) subsystem 12; (b) subsystem 3; (c), subsystem 4.
Vertical dash lines indicate the bandwidth of the 1 kHz octave band;

Figure 5. Energies of subsystem 3 (left) and subsystem 4 (right) for the 250 Hz, 500 Hz and 1 kHz octave bands and for damping loss factor values: (a) $\eta = 0.005$; (b) $\eta = 0.01$; (c) $\eta = 0.02$; (d) $\eta = 0.05$. Test case #1.

Figure 6. Maximum modal angular rotations at the coupling edge $\theta_p^{\max}$ versus modal frequency f_p. Cross: modes of the free subsystem 12 (like in DMF); Square: global modes of case #1; Circle: global modes of case #2.

Figure 7. Partitioning and boundary conditions for the second test: (a) Alternative DMF substructuring; (b) CB substructuring. (Section view of the panels).

Figure A.1. (a) Rigid coupling of two continuous subsustems; (b) Fictive separation of the two subsystems with the associated prescribed condition on the coupling surface Γ.

TABLE CAPTIONS

Table 1: Comparison of subsystem energies for test cases #1 and #2. Role of resonant and non-resonant modes. Results correspond to the 1 kHz octave band (dB, ref. 10^{-12}J).

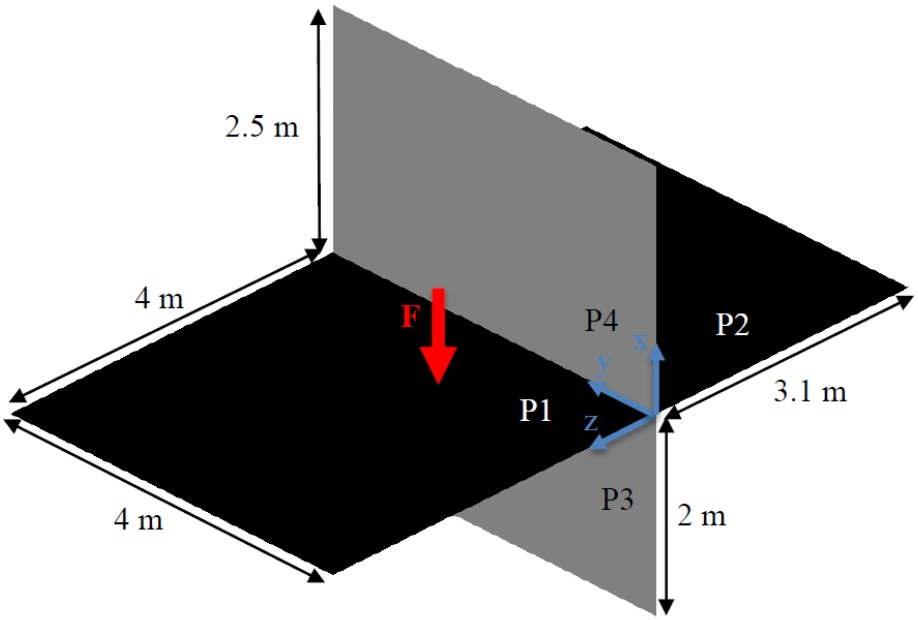

Figure 1. Geometry of the benchmark structure.

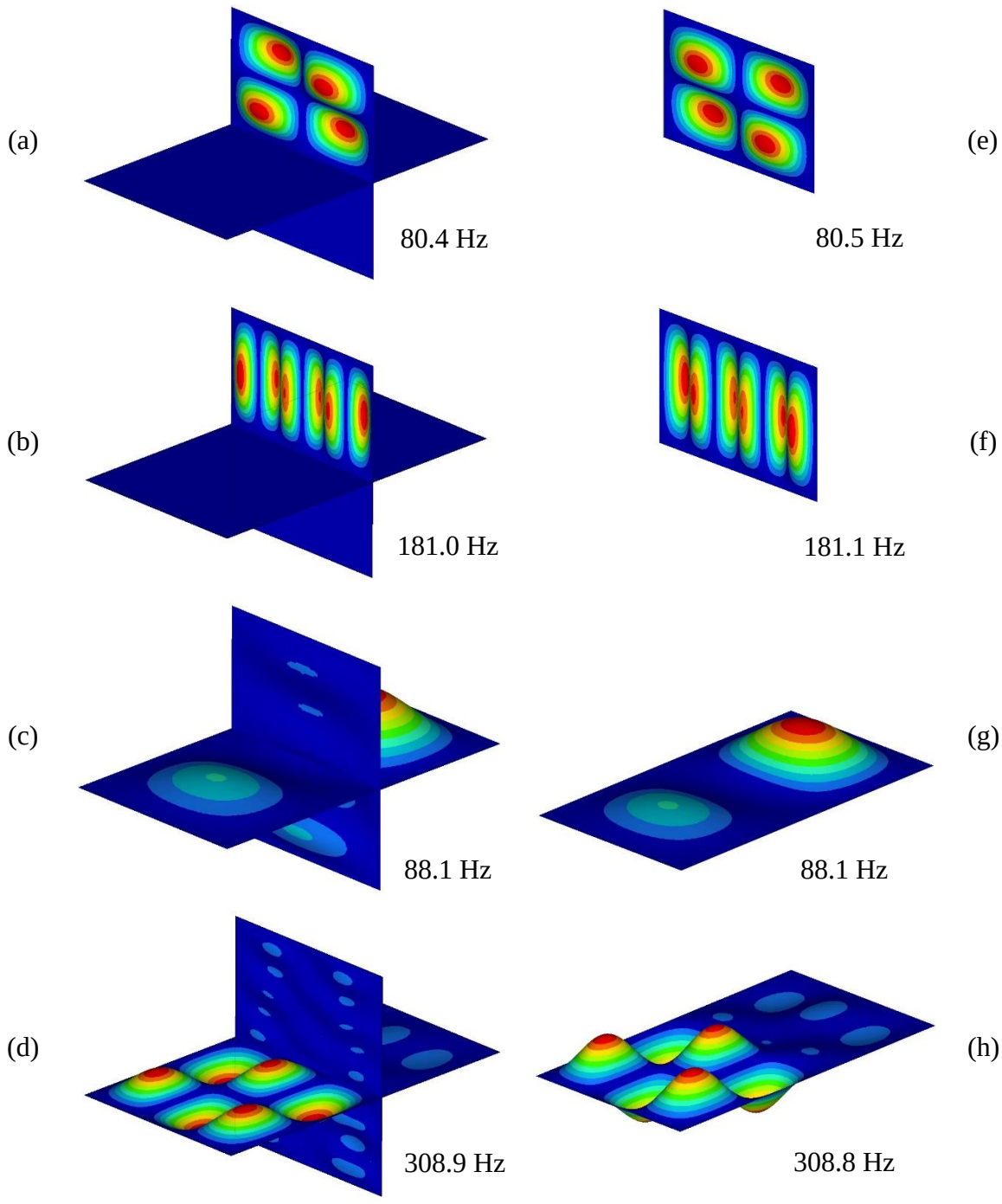

Figure 2. Comparison of the spatial shapes of the system global modes (left column) and the subsystem modes computed with the DMF (right column) for the first test case. (a-d) examples of global modes; (e-f) blocked modes of P4: (g-h) free modes of P1+P2.

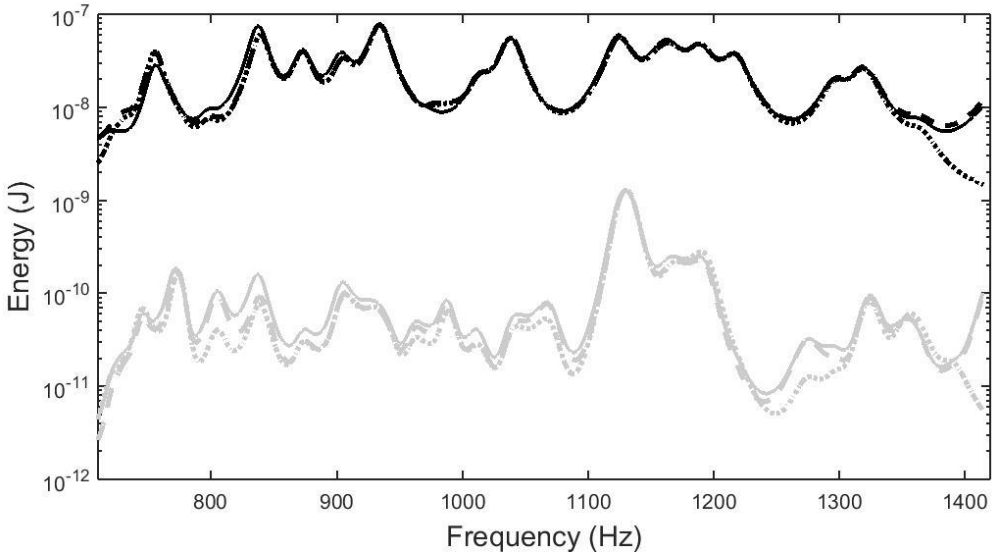

Figure 3. Subsystem energy response depending on frequency for subsystem 12 (black) and subsystem 3 (grey), for test case #1. Continuous line: reference energy from global modes; Dashed line: DMF computation considering resonant and non-resonant modes; Dotted line: DMF computation with only resonant modes.

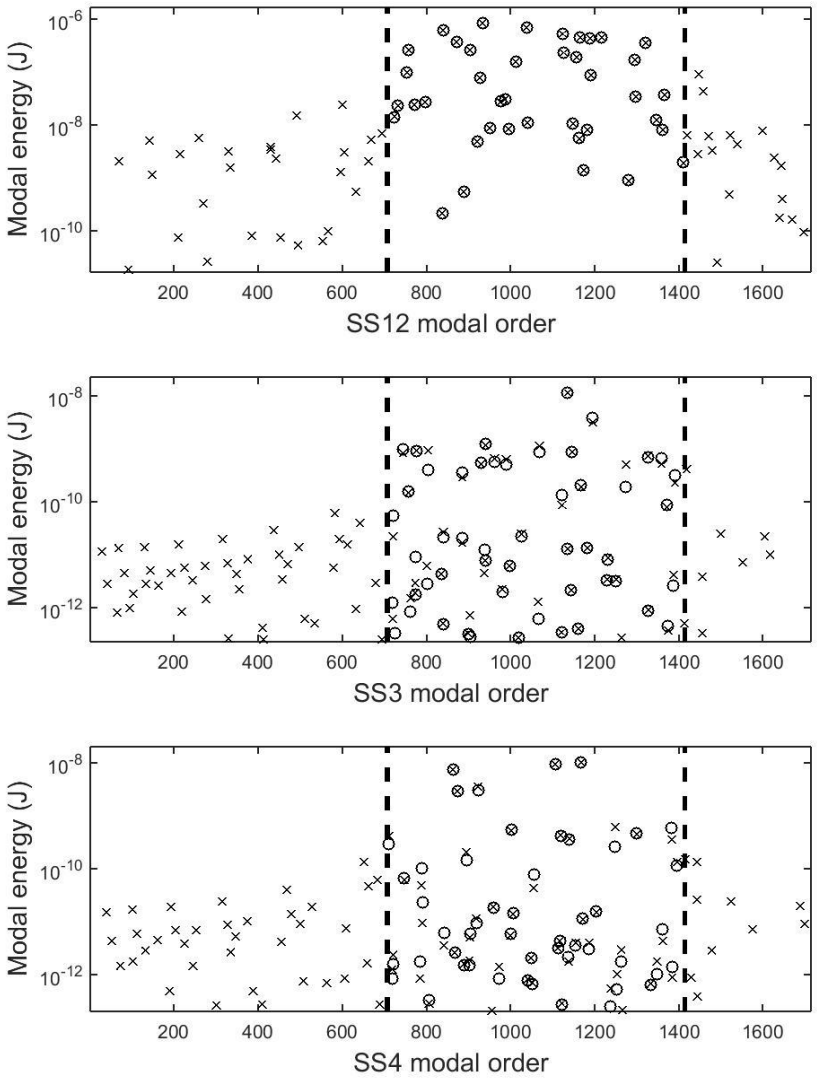

(a)

(b)

(c)

Figure 4. Modal energy distribution for test case #1. Cross: DMF taking into account resonant and non-resonant modes; Circle: DMF only considering resonant modes; (a) subsystem 12; (b) subsystem 3; (c) subsystem 4.

Vertical dash lines indicate the bandwidth of the 1 kHz octave band;

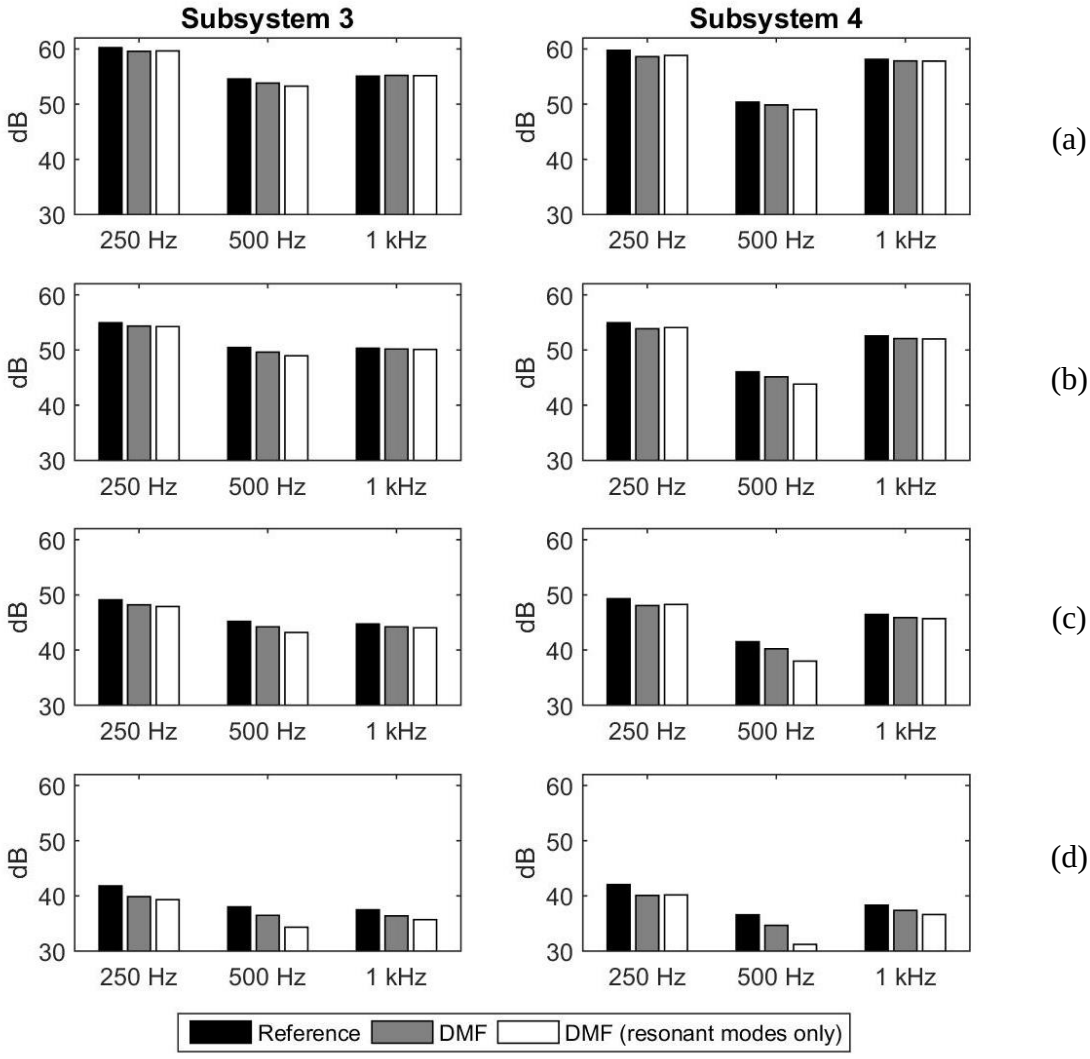

Figure 5. Energies of subsystem 3 (left) and subsystem 4 (right) for the 250 Hz, 500 Hz and 1 kHz octave bands and for damping loss factor values: (a) $\eta = 0.005$; (b) $\eta = 0.01$; (c) $\eta = 0.02$; (d) $\eta = 0.05$. Test case #1.

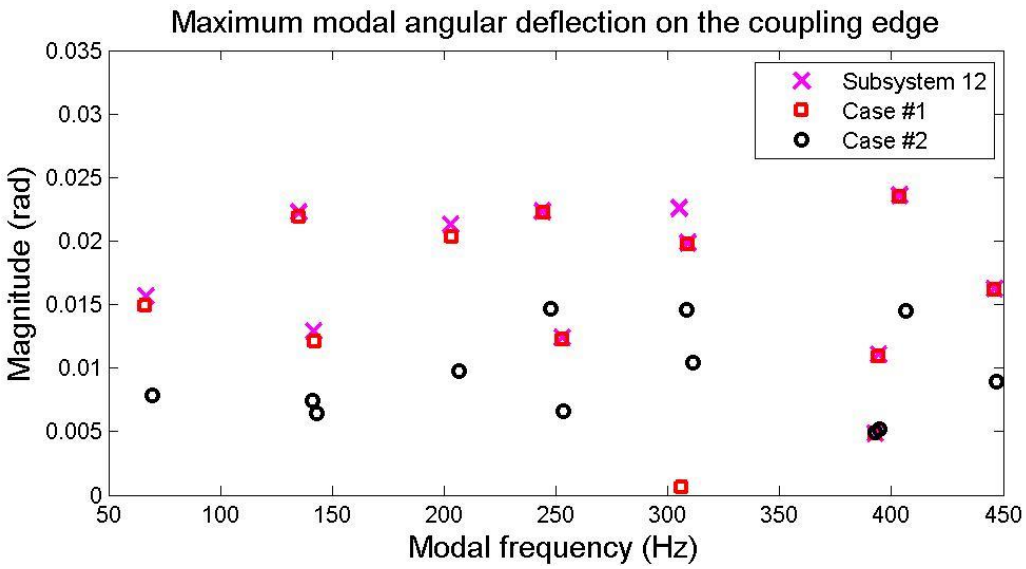

Figure 6. Maximum modal angular rotations at the coupling edge $\theta_p^{\max}$ versus modal frequency f_p. Cross: modes of the free subsystem 12 (like in DMF); Square: global modes of case #1; Circle: global modes of case #2.

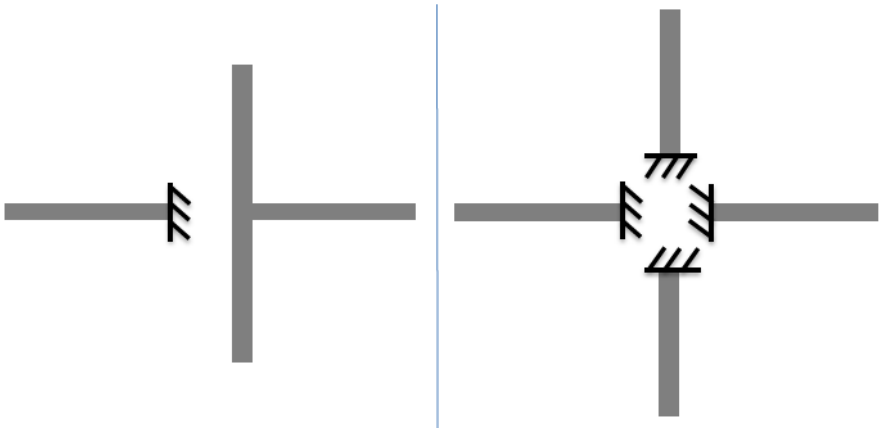

(a) (b)

Figure 7. Partitioning and boundary conditions for the second test: (a) Alternative DMF substructuring; (b) CB substructuring. (Section view of the panels).

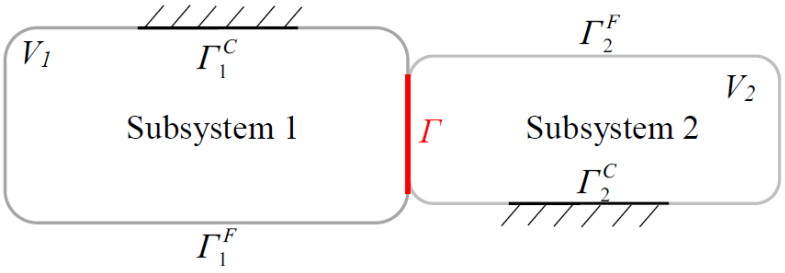

(a)

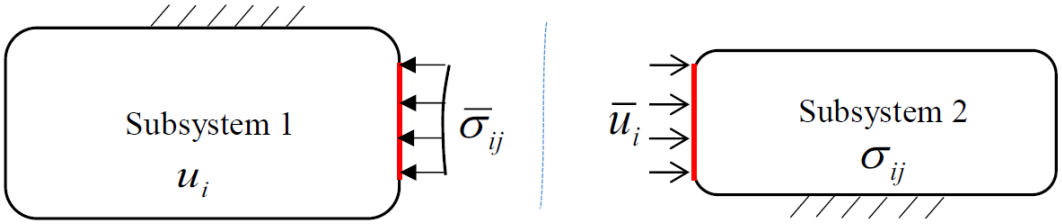

(b)

Figure A.1. (a) Rigid coupling of two continuous subsustems; (b) Fictious separation of the two subsystems with the associated prescribed conditions on the coupling surface Γ.